






# Enhancing urban flood hazard assessment: A comparative analysis of frequency ratio and xgboost models for precision risk mapping

Mohamed El Haou<sup>1\*</sup> , Malika Ourribane<sup>1</sup> , Maryem Ismaili<sup>1</sup> ,  
Samira Krimissa<sup>1</sup> , Mustapha Namous<sup>1</sup> 

<sup>1</sup> Data Science for Sustainable Earth Laboratory (Data4Earth), Faculty of Sciences and Technics, Sultan Moulay Slimane University, 23000 Beni Mellal, Morocco

\* Corresponding author's e-mail: [elhaou.mohamed@usms.ac.ma](mailto:elhaou.mohamed@usms.ac.ma)

## ABSTRACT

Urban flood hazard prediction should effectively balance accuracy and interpretability. This paper compares the performances of the Frequency Ratio method, a simple statistical technique, and XGBoost, a state-of-the-art machine learning algorithm for flood Hazard mapping in Beni Mellal (Morocco). The dataset was derived from preprocessed and standardized Sentinel-2 and Landsat 8 images, a Digital Elevation Model, and geological and soil maps. A flood inventory map was produced, it was then divided into training and testing subsets in the ratio of 70:30 for model calibration and validation, respectively. The FR method highlights key geographical variables such as slope, proximity to rivers, and vegetation indices to deliver rapid, interpretable flood risk assessments. In contrast, XGBoost captures complex, nonlinear relationships by integrating natural and anthropogenic factors for precise risk mapping. The results indicate that while FR is efficient for preliminary assessments in data-scarce environments, XGBoost significantly outperforms it in accuracy, reliability, and detailed hazard differentiation. XGBoost achieved an area under the curve (AUC) of 90.71% in testing datasets compared to 86.1% for FR. Flood distribution analysis showed that FR identified 21.3% of the study area as low-risk and 11.3% as very high-risk, suitable for broad evaluations. XGBoost, however, mapped 73.0% as very low-risk and 12.0% as very high-risk, making it valuable for resource-efficient interventions. This study highlights the complementary strengths of both approaches and advocates for integrating FR's rapid insights with XGBoost's precision. Together, they provide a robust framework for comprehensive flood hazard management in semi-arid regions, balancing strategic planning with localized interventions.

**Keywords:** urban flood; prediction, mapping; machine learning, statistical method; frequency ratio, xgboost, risk assessment.

## INTRODUCTION

The rapid and often unplanned growth of cities in areas vulnerable to natural disasters has significantly increased the risk of flooding, posing serious challenges for urban management and public safety (Beshir and Song, 2021; Eini et al., 2020). Floods lead to widespread social, economic, and environmental consequences, including damage to critical infrastructure, loss of personal property, and long-term impacts on affected communities (Alipour et al., 2020; Chen et al., 2015). Effective water resource management is critical

in urban settings where rapid development and climate change exacerbate flood risks (Abdrabo et al., 2020; Almouctar et al., 2024; Antzoulatos et al., 2022). As a result, proactive and integrated flood risk management strategies are essential to minimize immediate damages and mitigate broader socioeconomic impacts (Arabameri, Pal, et al., 2021; Taromideh et al., 2022).

Sustainable development frameworks, particularly those incorporating nature-based solutions (NBS), are gaining recognition in flood management. Initiatives such as urban reforestation and flood mitigation reservoirs demonstrate the

potential of NBS to regulate water flow and reduce peak flood events (Pirone et al., 2024). Lessons from Brazil's Cantareira system further emphasize the importance of sustainable water and soil management in mitigating flood risks (Lense et al., 2023). These combined approaches not only enhance flood resilience but also strengthen ecosystem adaptability in the face of climate change (Anaya-Romero et al., 2015; Mahmoud and Gan, 2018).

In 2019, the Council of Beni Mellal initiated a pivotal partnership aimed at enhancing flood protection measures for the city, allocating a budget of approximately \$7.8 million. This project underscores the city's commitment to proactive and integrated flood management, combining practical improvements with a forward-thinking approach to safeguarding its residents. Such efforts highlight the pressing need for innovative strategies that address both short-term risks and long-term sustainability.

Advances in technology, especially geographic information systems (GIS), remote sensing, and geophysical methods, have revolutionized flood risk management. For example, UAV-captured multispectral imagery has been used to assess riparian vegetation's role in streamflow regulation (Crimaldi and Lama, 2021). While geophysical techniques and hydrochemical analyses have aided in monitoring coastal aquifers (Bechkit et al., 2024). Emerging tools, such as fisheye lenses for assessing the leaf area index (LAI), provide deeper insights into vegetation's influence on local hydrology (Ismaili et al., 2024). Together, these technological advancements facilitate more accurate flood predictions and detailed hazard mapping, which are critical for preemptive risk management (Rahmati et al., 2016).

However, despite these advancements, traditional hazard mapping methods face persistent challenges, including limitations in data quality, difficulty accounting for climate change and rapid urbanization, and computational inefficiencies (Cea and Costabile, 2022). Machine learning techniques, such as random forest, have shown promise in addressing these challenges by improving flash flood susceptibility mapping in complex environments, as demonstrated in the Assaka watershed in southwestern Morocco (Talha et al., 2025). Additionally, urban and agricultural activities in flood-prone zones disrupt natural hydrological patterns, further complicating risk mitigation efforts (Ismaili et al., 2023;

Soussa, 2010). Case studies from vulnerable regions like the Middle East underscore the need for resilient, multidisciplinary approaches that integrate advanced and traditional techniques (Salmi and Al-Ghamdi, 2020).

Given these challenges, it is clear that flood hazard mapping techniques must evolve to integrate both traditional statistical methods and advanced machine learning approaches. This study evaluates the complementary roles of the frequency ratio (FR) method and the XGBoost machine learning algorithm in flood hazard mapping. The FR method, a simple statistical approach that uses historical data, provides intuitive and interpretable insights into flood-contributing factors, making it suitable for broad-scale assessments with limited computational resources. XGBoost, on the other hand, is a state-of-the-art machine learning algorithm known for its ability to handle complex datasets and model nonlinear interactions, offering higher precision in identifying critical flood zones.

This research compares these two complementary methods of flood hazard mapping using the same dataset, composed of environmental variables derived from Sentinel-2 and Landsat 8 satellite imagery, a digital elevation model, and geological and soil maps. The goal is to assess their effectiveness in quantifying flood risks in urban environments. Specifically, it aims to:

1. Establish the complementarity of statistical and machine learning methods for flood hazard assessment.
2. Develop a robust framework that integrates interpretability (from FR) and precision (from XGBoost) to improve flood risk prediction.
3. Provide a reliable flood hazard assessment methodology tailored to urban environments in semi-arid regions like Beni Mellal.

This study hypothesizes that XGBoost will surpass the FR method in predictive accuracy, given its capacity to model nonlinear interactions and handle large datasets. However, the FR method is expected to offer valuable insights into the direct contributions of flood-conditioning factors, making it an effective tool for strategic planning. By combining these methods, the research seeks to enhance both the understanding of flood dynamics and the reliability of flood risk mapping in semi-arid urban areas. The findings will inform resilient urban planning in Beni Mellal and contribute to global efforts toward sustainable flood

risk management in similar regions facing increasing climate risks.

## MATERIALS AND METHODS

### Study area and data description

The research site is situated in the city of Beni Mellal, a metropolitan area located in the central region of Morocco. The study area extends approximately between 32°18'30"N to 32°22'50"N latitude and 6°27'0"W to 6°18'20"W longitude (Figure 1) encompassing an area of 53.32 km<sup>2</sup>. This city holds significant economic, cultural, and social significance in the area. Beni Mellal is distinguished by its expanding urban growth and a clustering of population, infrastructure, agricultural, and industrial pursuits. This expansion has presented difficulties in managing natural resources and adapting to severe weather events like flooding (Barakat et al., 2020).

Geographically, the Beni Mellal region is mountainous, with elevations ranging from 470 m to 2247 m, the highest point being Tassemit. The area's climate is labeled as continental, with an average temperature of approximately 18 °C. Annual rainfall averages 490 mm, with July being the driest month and March the wettest, with an average precipitation of 79 mm. The study area's geographical, geological, topographical,

and climatic features create conditions favorable to flooding. Moreover, uncontrolled urban growth, changes to water systems, and population expansion have all played a role in altering the area's natural water flow. As a result, the frequency and severity of flooding events have changed, causing disruptions to residents' daily lives and putting strain on sanitation and stormwater systems (Cea and Costabile, 2022).

### Methodology

The methodology of the research includes three major steps: data collection and preparation, model development and training, and evaluation and mapping. Slope, land use, TWI, and NDVI environmental factors were obtained from Sentinel-2 and Landsat 8 images, a DEM, and geological and soil maps of the study area. The flood inventory was developed by applying the Normalized Difference Flood Index (NDFI) to Sentinel-2 images. The dataset was preprocessed, standardized, and split, allocating 70% for training and 30% for testing.

The machine learning model XGBoost and the FR statistical method were trained and tested. Their performance was evaluated using metrics such as AUC, Kappa, RMSE, MAE, and accuracy. The output of this process generated a flood susceptibility map, highlighting high-risk zones within the study area (Figure 2).

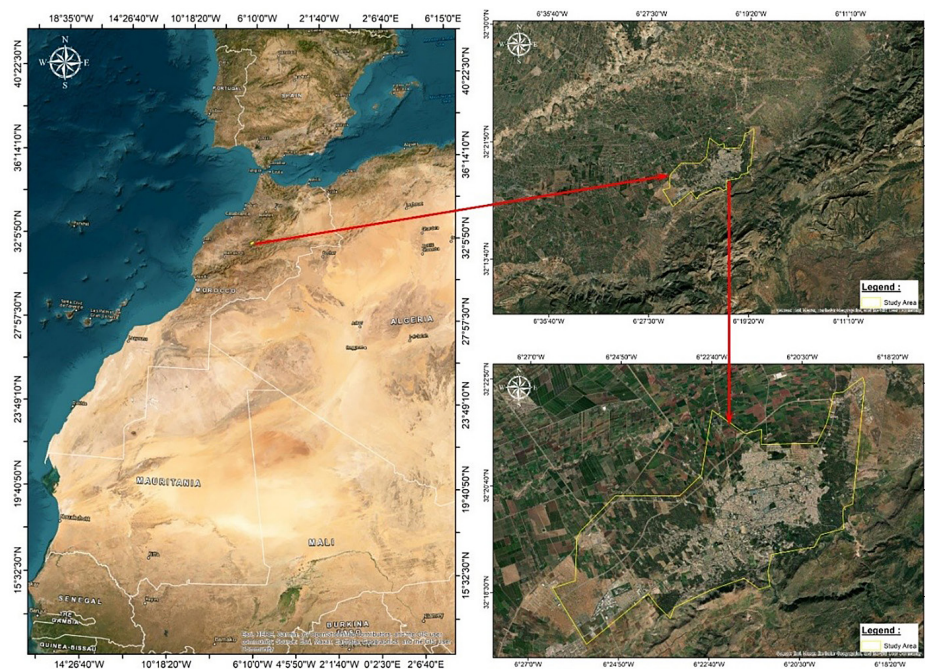


Figure 1. The geographical localization of the study area in Moroccan and regional context

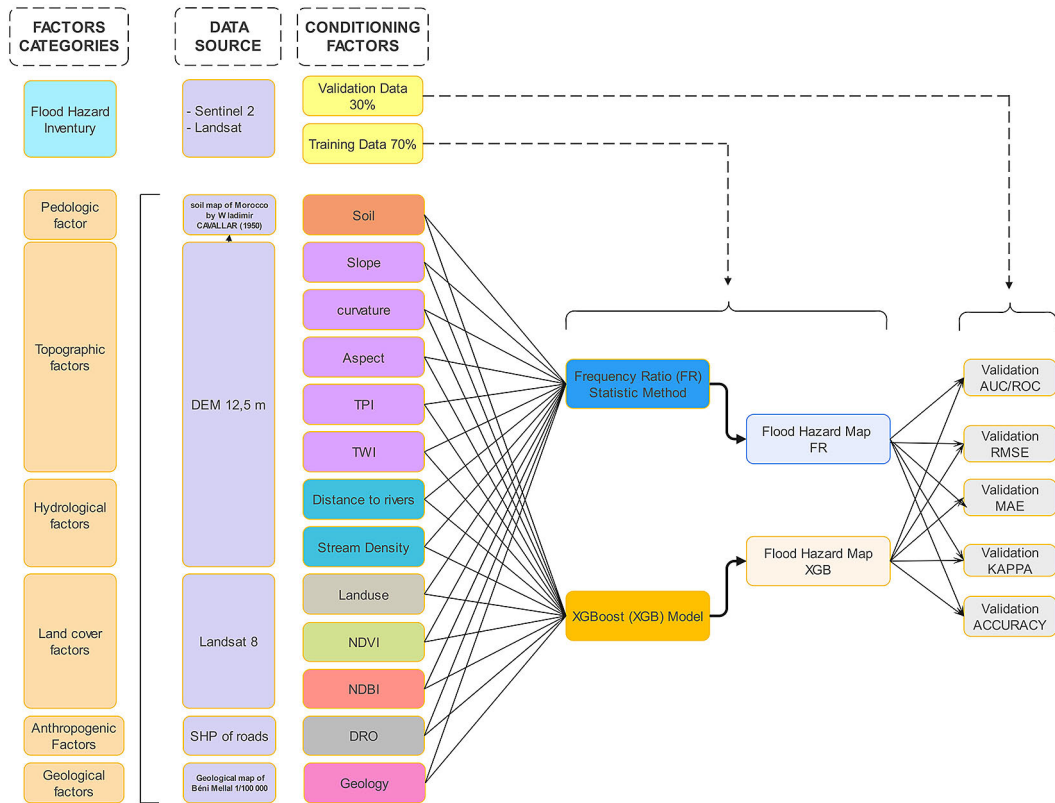


Figure 2. Flow chart of methodology developed in this study

Urban flood inventories

To forecast locations susceptible to flooding, it is essential to examine areas that have previously experienced flooding. To compiling the inventory for this research, Sentinel-2 satellite imagery was utilized to collect sample points during the flood event (Figure 3). These sample points were extracted from both peak flood and post-flood images. Water pixels were identified through the application of the normalized

difference flood index (NDFI), which was computed from images available in Google Earth Engine (GEE). The index values were derived using the equation established by Boschetti et al. (2014). A threshold of ‘0’ was implemented to mask pixels with values exceeding zero. This image thresholding method resulted in the generation of a binary map that visually distinguishes between flooded and non-flooded regions. Areas at risk of flooding were designated as “1,” while non-flooded areas were labeled as “0,” based on

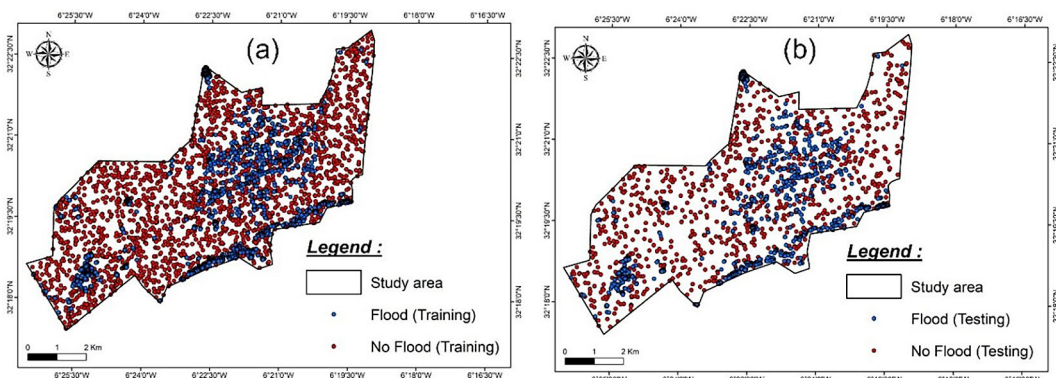


Figure 3. Historical flood events recorded between January 1, 2002, and December 1, 2020, which were tracked using the Sentinel-2 and Landsat satellites: (A) Distribution of training inventories; (B) Distribution of testing inventories

binary maps and a specific cut-off criterion. A flood inventory map was produced utilizing 2512 flood points. The dataset was then divided into two distinct categories: training and testing. Our literature review indicated that approximately 70% (2178 points) of a random subset was allocated for training and calibration purposes, while the remaining 30% (934 points) was reserved for validation (Figure 4).

### Conditioning factors

Several factors related to flooding were incorporated into the creation of predictive models to assess flood hazard, including geology, soil composition, NDVI, land use, slope, aspect, stream density, topographic position index (TPI), topographic wetness index (TWI), proximity to rivers, normalized difference built-up index (NDBI), and distance to roads (DRO).

### Geology

The examination of geology, which includes both the soil and the underlying rock types, has a significant influence on the flooding of watershed basins (Yang et al., 2020). This is primarily due to its direct effect on permeability and surface runoff. Figure 5i, depicting the geology map of the study area (Fig. 5I), was created using the 1:100,000 geological map of Beni Mellal, Morocco. The area's geology was classified into multiple units, such as pink-brown carbonated cement powders, travertines, Paleocene beige limestone, Middle Quaternary scree spreading, Recent Quaternary

piedmont cones (encrusted), and Middle Quaternary Tadla silts (Barakat et al., 2020).

### Soil

Soil moisture plays a critical role in predicting flood characteristics, especially in the summer months (Luong et al., 2021). The soil types map (Fig. 5m) within our study area is sourced from the esteemed soil map of Morocco, created by Vladimir Cavallar, also known as Kavaleridzé. Professor-Doctor Cavallar, a renowned expert in pedology from the Ukrainian Agronomic Institute, carried out this task on behalf of the National Center for Scientific Research (Centre National de la Recherche Scientifique) and the Agricultural Research Center of Morocco (Centre de Recherches Agronomiques du Maroc). This comprehensive map showcases the diverse range of soils in our region, including podzolic soils, podzolized red and brown soils, red soils, brown soils, and humus-carbonate soils found in forested areas.

### NDVI

The normalized difference vegetation index (NDVI), holds significant importance in evaluating vegetation, where positive values signify the presence of dense vegetation (Fig. 5e). This assessment is essential in understanding the effects of floods, as dense vegetation, identified by high NDVI values, plays a crucial role in mitigating flood risks by promoting water infiltration and minimizing surface runoff. Moreover, it serves as a safeguard against erosion and aids in fortifying



**Figure 4.** Photos illustrating the floods and small watersheds crossing the city of Beni Mellal

riverbanks (Atefi and Miura, 2022). The NDVI is determined through the following Equation 1 below:

$$NDVI = \frac{NIR - R}{NIR + R} \quad (1)$$

where: NIR and R are the spectral reflectance of the near infrared and red bands, respectively.

#### Land use

Land use and its extent play a significant role in influencing surface water flow, infiltration rates, and evapotranspiration processes within a given region (Rahman et al., 2021). These factors, in turn, directly or indirectly affect the likelihood of flooding. Using supervised classification of Landsat 8 data, the study area was categorized into four distinct land use and land cover types: Built-up, Arboriculture, Agricultural Land and Bare ground (Fig. 5k).

#### Slope

Another important physical factor influencing flooding is slope. Generally, the steepness of a slope affects the speed of water movement and discharge (Nguyen et al., 2020). This factor was derived from the digital elevation model (DEM) and categorized into five segments (Fig. 5i).

#### Aspect

The orientation of a slope affects several environmental elements, such as the distribution of rainfall, soil moisture, and exposure to solar radiation, which ultimately have an indirect impact on surface runoff (Peng et al., 2020). Slope Aspect refers to the direction that a terrain surface inclines towards and is measured in degrees, rotating clockwise from 0° (north) to 360° (north again) (Pham et al., 2019). For the purpose of this analysis, slope aspects are categorized into flat, north, northeast, east, southeast, south, southwest, west, and northwest (Fig. 5a).

#### Curvature

Curvature (Fig. 5f) is defined as the rate at which the slope gradient changes and can be categorized as either profile curvature or plan curvature (Raja et al., 2017). Profile curvature has an impact on the speed changes of flow across a surface, influencing erosion and deposition activities. On the other hand, plan curvature affects the convergence

and divergence of flow, impacting the flow path and water accumulation. The mean curvature, which combines profile and plan curvature, can reflect important topographic features such as ridge lines, valley lines, platform edges, and wide valley edges.

#### Stream density

The stream density (Fig. 5c) was established by computing the combined length of all streams and dividing it by the drainage basin's area (Bogale, 2021). Typically, an elevated stream density signifies a heightened risk of flooding caused by greater surface runoff. This is due to the fact that regions with high stream density expedite the flow of surface runoff, making them more vulnerable to flooding incidents.

#### TPI

The topographic position index (TPI), also known as relative topography, measures the variation in elevation between a central cell and the surrounding cells on the terrain surface (Avand et al., 2022). A positive TPI indicates that the cell is located at a higher elevation than its surroundings, indicative of features such as ridges (Fig. 5j), while negative values suggest that it is lower, characteristic of valleys. The TPI is calculated using Equation 2 below:

$$TPI = T_0 - \sum^{(n-1)} T_n \quad (2)$$

where:  $T_0$  represents the elevation of the cell being evaluated,  $T_n$  refers to the elevation values of the surrounding grid cells, and 'n' denotes the total number of cells in the specified neighborhood around the cell under evaluation.

#### TWI

The TWI (Figure 5d) quantifies the distribution of soil moisture across landscapes by combining slope and the area contributing upstream to comprehend the dynamics of water dispersal (Winzeler et al., 2022). The TWI is calculated using Equation 3 below:

$$TWI = \ln(A - \tan(\beta)) \quad (3)$$

where: A denotes the area of the local upslope contributing to drainage at a specific point, measured per unit of contour length, referred to as the specific catchment area or upstream contributing area;  $\tan(\beta)$  is the tangent of the slope angle ( $\beta$ ), indicating the terrain's steepness.

Distance to rivers

The distance from the river was determined using the GIS software’s distance tool, as shown in (Fig. 5h). This important measure indicates the distance between different land areas and the nearest body of water, which is significant for understanding the potential impact of water courses and resulting floods (Ibrahim et al., 2024). Additionally, the river network was obtained through the DEM processing using the Euclidean function within the GIS environment.

NDBI

The normalized difference built-up index (NDBI) (Fig. 5b) makes use of the near infrared (NIR) and short-wave infrared (SWIR) bands to emphasize urban or built-up areas. In these areas, as well as in bare soil regions, there is greater reflection in the SWIR band compared to the NIR band. Conversely, water bodies, which do not reflect well in the infrared spectrum, are easily distinguishable from built-up areas when using this index (Khan et

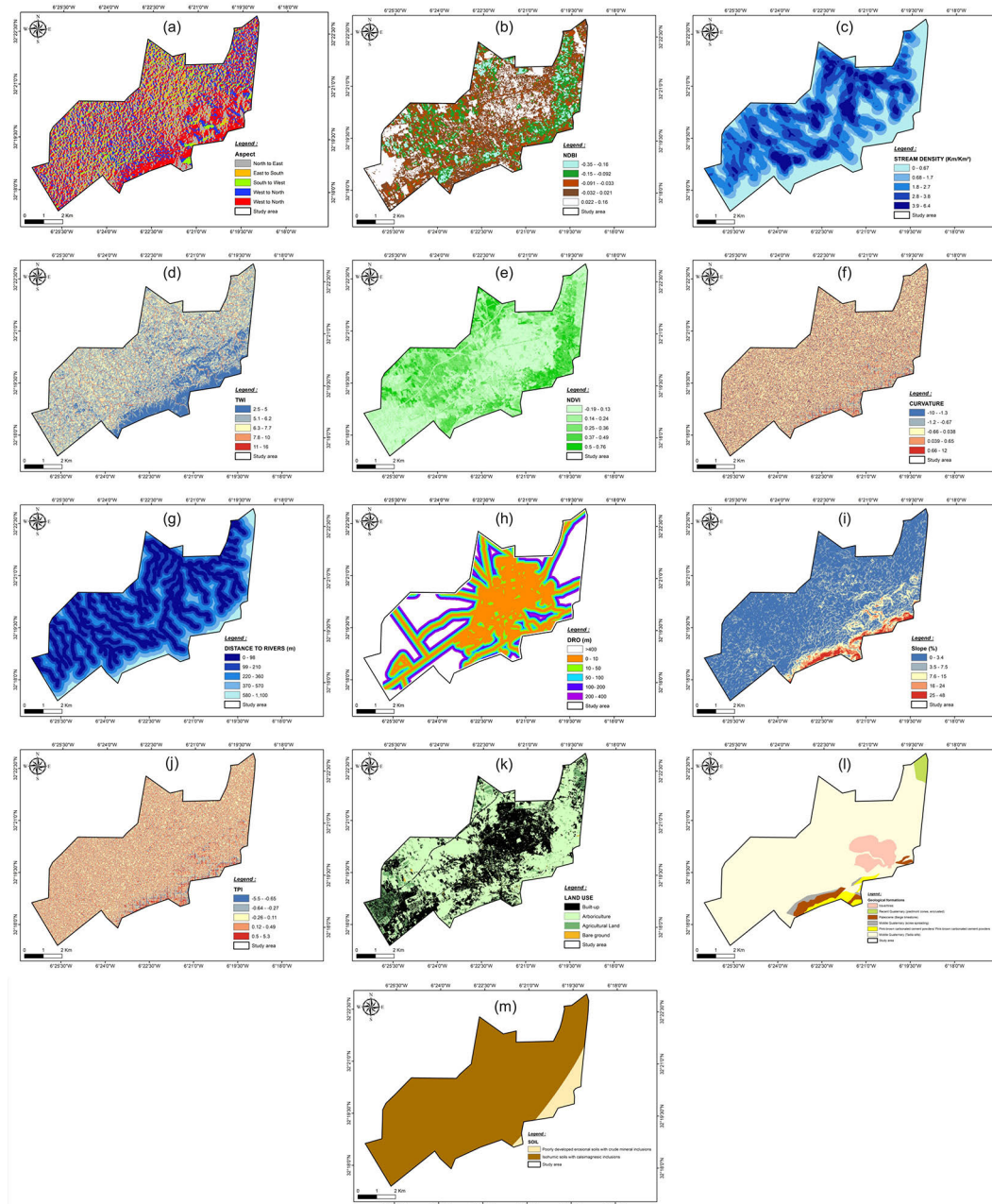


**Figure 5.** Flood influencing factors considered in the present study: (a) aspect, (b) NDBI, (c) stream density, (d) TWI, (e) NDVI, (f) curvature, (g) distance to rivers, (h) distance to roads (DRO), (i) SLOPE, (j) TPI, (k) land use, (l) GEOLOGY, (m) SOIL

al., 2021). This index is frequently utilized to evaluate the presence and extent of built-up areas, which may contribute to increased flood hazard due to impervious surfaces reducing water infiltration. NDBI is calculated using Equation 4:

$$NDBI = \frac{SWIR - NIR}{SWIR + NIR} \quad (4)$$

The values of the NDBI fall within a range of -1 to +1. A negative NDBI value is indicative of water bodies, whereas higher values are indicative of built-up areas. Vegetation usually demonstrates low NDBI values.

#### Distance to road (dro)

The proximity of roads plays a crucial role in contributing to flood hazard, as depicted in (Fig. 5h). This is due to the impervious surfaces commonly found on roads, which intensify runoff and reduce the soil’s capacity to absorb water, consequently elevating the risk of flooding (Rahman et al., 2021).

### Model selection and training

#### Frequency ratio

The frequency ratio model measures the connection between the spatial distribution of floods and their contributing environmental variables (Allouche et al., 2006; Tehrany et al., 2019). The frequency ratio for variables like elevation or slope is calculated by dividing the proportion of flood occurrences by the area proportion of each variable, according to Equation 5. A higher bivariate probability (greater than 1) indicates a stronger association between flood occurrences and the contributing factors, whereas a lower probability (less than 1) indicates a weaker association (Yalcin et al., 2011). The flood hazard map of FR model is generated by the following Equation 6 in ESRI ArcGIS:10.8 software.

$$FR = \frac{\text{Pourcentage of flood (PL)}}{\text{Pourcentage of the class of each conditioning factor (PD)}} \quad (5)$$

$$\begin{aligned} \text{Flood Hazard (FR)} = & FR_{Aspect} \times Aspect + FR_{Slope} \times Slope + FR_{Curvature} \times \\ & Curvature + FR_{Soil} \times Soil + FR_{TPI} \times TPI + FR_{TWI} \times TWI + FR_{Distance\ to\ rivers} \times \\ & Distance\ to\ rivers + FR_{Land\ Use} \times Land\ Use + FR_{Stream\ Density} \times Stream\ Density + \\ & FR_{Geology} \times Geology + FR_{NDVI} \times NDVI + FR_{NDBI} \times NDBI + FR_{DRO} \times DRO \end{aligned} \quad (6)$$

#### XGBoost

In the XGBoost is boosting ensemble learning methods (Ren et al., 2024). It is a variation of Gradient Boosting Trees that enhances the gradient boosting algorithms capabilities while improving computing efficiency and accuracy. The XGBoost method has numerous novel features based on decision tree algorithms, such as automatically altering the order in which decision trees are constructed to reduce errors. It also employs regularization approaches to reduce overfitting and increase the model generalizability. The XGBoost algorithm has several changeable parameters, including the learning rate, tree depth, and regularization parameters, requiring some tuning skill. The XGBoost technique is highly computationally efficient.

#### Training and validation

Validation and optimization are essential in predictive modeling to ensure reliable and consistent results (Bouramtane et al., 2022). Without proper validation, the outputs of machine learning models hold limited practical significance (Arabameri et al., 2021).

In this study, we used RStudio to assess model performance through metrics such as AUC/ROC, Cohen’s Kappa, RMSE, MAE, and accuracy. The dataset was divided into training (70%) and testing (30%) subsets to train and evaluate the models effectively. The FR statistical method and the XGBoost machine learning algorithm were applied separately to compare their strengths.

XGBoost was trained using standardized controls with 10-repeated 10-fold cross-validation, excelling in binary logistic classification. The FR method relied on historical flood data and environmental variable correlations to identify flood-prone areas. Both approaches demonstrated promising results for urban flood prediction, each showcasing unique strengths in reliability and precision (Table 1).



**Table 1.** Parameters and settings for machine learning model (XGBoost)

Model	Parameter	Value	Description
XGBoost	Objective	"binary:logistic"	Binary classification model
	Max_depth	4	Maximum depth of the trees
	Eta	0.2	Learning rate controlling the step size for updates
	Subsample	0.8	Proportion of rows used for training each tree
	Colsample_bytree	0.8	Proportion of columns used for training each tree
	Gamma	1	Regularization term to penalize overly complex trees
	Min_child_weight	10	Minimum sum of instance weights (hessian) needed in a child

*Auc/roc*

Before creating the models, we evaluated the performance of different prediction methods using the receiver operating characteristic-area under the curve (ROC-AUC) metric on test data. The ROC curve is a key tool in spatial modeling that visually demonstrates the balance between specificity and sensitivity. Here’s a simplified breakdown of its main elements:

- Specificity: Plotted on the x-axis, it shows how well the model correctly identifies areas that are not prone to flooding. It’s calculated as the percentage of true negatives (correctly predicted non-flood points) out of all non-flood observations.
- Sensitivity: Plotted on the y-axis, it’s also called recall or the true positive rate. This measures how effectively the model identifies flood-prone areas, showing the proportion of actual flood locations correctly predicted.
- Area under the curve (AUC): This is a single value that summarizes the ROC curve’s ability to separate flood-prone and non-flood-prone areas. AUC values range from 0 to 1, with higher values indicating better model performance in distinguishing between the two categories, where:
  - 0 represents a model with no discriminative ability,
  - 0.5 suggests a performance no better than random chance,
  - 1 indicates perfect classification.

The AUC is calculated using Equation 7 below:

$$AUC = \frac{(\sum TP + \sum TN)}{P + N} \tag{7}$$

where:  $\sum TP$  (sum of true positives) – the total number of flood locations correctly identified as flood;  $\sum TN$  (sum of true negatives)

– the total number of non-flood locations correctly identified as non-flood;  $P$  (positives) – the total number of actual flood locations (pixels with torrential phenomena);  $N$  (negatives) – the total number of actual non-flood locations (pixels without torrential phenomena).

This equation effectively reflects the ratio of accurate outcomes (including both true positives and true negatives) relative to the overall number of cases assessed, offering an indication of the model’s precision in accurately classifying each pixel. This thorough assessment aids in identifying the most efficient models to incorporate into an ensemble for enhanced predictive capabilities.

*Mae (mean absolute error)*

MAE is valuable when predicting quantitative aspects of flooding, such as water levels or flow rates at specific gauge stations. It gives an average of the absolute errors between predicted values and observed values, providing a clear measure of prediction error in the same units as the prediction itself (Haghizadeh et al., 2017; Janizadeh et al., 2021).

The equation for MAE is:

$$MAE = \frac{1}{n} \sum_{i=1}^n |y_i - \hat{y}_i| \tag{8}$$

where:  $n$  is the number of observations;  $y_i$  is the actual (observed) value for the  $i$ -th observation;  $\hat{y}_i$  is the predicted value for the  $i$ -th observation;  $|y_i - \hat{y}_i|$  is the absolute difference between the actual and predicted values.

*Rmse (root mean square error)*

RMSE is particularly effective for quantitative forecasts, such as predicting water levels or flow rates. Its value lies in the way it disproportionately

penalizes larger errors over smaller ones. This attribute is critical in flood prediction, where underestimating the impact of an event can have more severe consequences than overestimating it (Haghizadeh et al., 2017; Janizadeh et al., 2021).

These metrics can help determine how reliable and accurate a flood prediction model is in practical scenarios. Moreover, they can guide improvements in model development and deployment, ensuring better preparedness and response strategies for flood-prone areas (Haghizadeh et al., 2017; Janizadeh et al., 2021).

The equation for RMSE is:

$$RMSE = \sqrt{\frac{1}{n} \sum_{i=1}^n (y_i - \hat{y}_i)^2} \quad (9)$$

where:  $n$  is the number of observations;  $y_i$  is the actual (observed) value for the  $i$ -th observation;  $\hat{y}_i$  is the predicted value for the  $i$ -th observation;  $(y_i - \hat{y}_i)$  is the squared difference between the actual and predicted values.

### Kappa

Cohen’s Kappa is a statistical tool that measures the agreement between two sets of rankings or predictions, while taking into account the probability of agreement obtained simply by chance. This measure is particularly relevant in the evaluation of prediction models, especially those that generate categorical results, as in the validation of flood forecasts. In flood prediction, Cohen’s Kappa can be used to assess the performance of different models and measure inter-rater reliability (Paul et al., 2022)

The equation for Kappa (Cohen’s Kappa) is:

$$k = \frac{p_o - p_e}{1 - p_e} \quad (10)$$

where:  $p_o$  is the observed agreement, which is the proportion of times the two raters (or the model and ground truth) agree;  $p_e$  is the expected agreement, which is the proportion of times the two raters (or model and ground truth) would agree by chance.

### Accuracy

Accuracy is a straightforward measure when predicting whether a flood will occur or not (binary classification: flood/no flood). It provides a quick snapshot of overall model effectiveness but can be misleading if the data set is unbalanced

(e.g., very few flood events compared to non-flood days). The equation for accuracy is:

$$Accuracy = \frac{TP + TN}{TP + TN + FP + FN} \quad (11)$$

where:  $TP$  (true positives) – the number of correctly predicted flood events;  $TN$  (true negatives) – the number of correctly predicted non-flood events;  $FP$  (false positives) – the number of non-flood events incorrectly predicted as floods;  $FN$  (false negatives) – the number of flood events incorrectly predicted as non-floods.

## RESULTS

### Importance of variables and analysis of explanatory factors using statistical method

The analysis of flood hazard involves various factors that contribute to the overall risk. Table 2 provides a comprehensive breakdown of these factors, categorized by classes such as aspect, slope, curvature, soil, TPI, TWI, distance to rivers, land use, stream density, geology, NDVI, NDBI, and DRO. Each class is analyzed based on frequency ratio (FR) index. These indices help to normalize the data and provide a clear picture of the relative importance of each class in predicting flood hazards. In the following sections, we will classify and discuss these classes according to the three different prediction models used in this study.

The frequency ratio method pays more attention to slope, appearance and NDVI. These results reveal a significant agreement, especially with regard to the importance of slope and vegetation, while highlighting the particularities of each method. It is essential to recognize the uniqueness of the FR method; although it may seem simple, it highlights geographical factors that are often ignored, making it a valuable and essential tool for in-depth and relevant analyses

### Importance of variables and analysis of explanatory factors using machine learning model XGBoost

In the analysis performed with XGBoost, it is clearly demonstrated that the most influential variables are NDVI, NDBI and SLOPE (Figure 6). This highlights the crucial importance of vegetation indices and topography in our understanding of the phenomena studied.

**Table 2.** Spatial relation between thematic layers and historic floods using FR method

Factor	Class	Nbr. of Pixel	% of domain	Nbr. of inundation points	% Flood	FR index	FR normalized
Aspect	North to East	93350	27.68	533	24.46	0.88	0.88
	East to South	39590	11.74	213	9.78	0.83	0.05
	South to West	47047	13.95	198	9.09	0.65	0.04
	West to North	68096	20.19	280	12.85	0.63	0.04
	West to North	89171	26.44	955	43.83	1.65	0.11
Slope (%)	0–3.36	216201	64.11	883	40.52	0.63	0.04
	3.36–7.48	86644	25.69	542	24.87	0.96	0.06
	7.48–14.78	18986	5.63	85	3.90	0.69	0.04
	14.78–24.33	9864	2.92	141	6.47	2.21	0.15
	24.33–47.73	5559	1.65	528	24.23	14.7	1.00
Curvature	-10.23–1.29	56699	16.81	395	18.13	1.07	0.07
	-1.29–0.67	161642	47.93	947	43.46	0.90	0.06
	-0.67–0.03	63508	18.83	395	18.13	0.96	0.06
	0.03–0.65	47764	14.16	291	13.35	0.94	0.06
	0.65–9.60	7641	2.27	151	6.93	3.05	0.20
SOL	Poorly developed erosional soils with crude mineral inclusions	269635	79.95	1411	64.75	0.81	0.05
	Isohumic soils with calsimagnesian inclusions	67619	20.05	768	35.25	1.75	0.12
TPI	-5.5–0.65	19438	5.76	109	5.00	0.86	0.05
	-0.65–0.27	88554	26.26	407	18.68	0.71	0.04
	-0.27–0.10	121760	36.10	665	30.52	0.84	0.05
	0.10–0.48	89179	26.44	628	28.82	1.09	0.07
	0.48–5.25	18323	5.43	370	16.98	3.12	0.213
TWI	2.504–4.97	51729	15.34	884	40.57	2.64	0.18
	4.97–6.18	175009	51.89	837	38.41	0.74	0.05
	6.18–7.71	84166	24.96	352	16.15	0.64	0.04
	7.71–10.18	18280	5.42	69	3.17	0.58	0.04
	10.18–15.92	8070	2.39	37	1.70	0.71	0.04
Distance to rivers (m)	0–98.37	133496	39.58	624	28.64	0.72	0.04
	98.37–210.16	102770	30.47	512	23.50	0.77	0.05
	210.16–357.72	60860	18.05	309	14.18	0.78	0.05
	357.72–567.88	27446	8.14	396	18.17	2.23	0.15
	567.88–1 140.24	12682	3.76	338	15.51	4.12	0.28
Land use	Built-up	132323	39.24	1367	62.74	1.59	0.10
	Arboriculture	181601	53.85	756	34.69	0.64	0.04
	Agricultural land	22042	6.54	54	2.48	0.37	0.02
	Bare ground	1288	0.38	2	0.09	0.24	0.01
Stream Density (km/km <sup>2</sup> )	0–0.67	73600	21.82	907	41.62	1.90	0.13
	0.67–1.69	61794	18.32	365	16.75	0.91	0.06
	1.69–2.69	96653	28.66	406	18.63	0.65	0.04
	2.696945842–3.845644996	72262	21.43	334	15.33	0.71	0.04
	3.84–6.36	32945	9.77	167	7.66	0.78	0.05

Geology	Travertines	21224	6.29	171	7.85	1.24	0.08
	Recent Quaternary (piedmont cones. encrusted)	5255	1.56	3	0.14	0.08	0.00
	Paleocene (beige limestone)	9096	2.70	153	7.02	2.60	0.17
	Middle Quaternary (scree spreading)	4092	1.21	23	1.06	0.87	0.05
	Pink–brown carbonated cement powders/ Pink–brown carbonated cement powders	7057	2.09	332	15.24	7.28	0.49
	Middle Quaternary (Tadla silts)	290530	86.15	1497	68.70	0.79	0.05
NDVI	-0.19–0.13	36687	10.88	1275	58.51	5.37	0.36
	0.13–0.23	58162	17.25	487	22.35	1.29	0.08
	0.23–0.35	90248	26.76	313	14.36	0.53	0.03
	0.35–0.49	93618	27.76	99	4.54	0.16	0.01
	0.49–0.75	58539	17.36	5	0.23	0.01	0.00
NDBI	-0.34–0.15	24976	7.41	16	0.73	0.09	0.00
	-0.15–0.09	60064	17.81	97	4.45	0.25	0.01
	-0.09–0.03	72531	21.51	557	25.56	1.18	0.08
	-0.03–0.02	100035	29.66	940	43.14	1.45	0.09
	0.02–0.16	79648	23.62	569	26.11	1.10	0.07
DRO (m)	0–10	213902	63.42	1641	75.31	1.18	0.08
	10–50	97360	28.87	508	23.31	0.80	0.05
	50–100	23871	7.08	30	1.38	0.19	0.01
	100–200	2121	0.63	0	0.00	0.00	0.00
	200–800	0	0.00	0	0.00	0.00	0.00

### Impact of classes in prediction

The biggest factor influencing flood hazards (Figure 7) in FR model is steep slopes (24.33–47.73%), which cause high erosion and runoff. Next is the north to east slope orientation. Areas with pink-brown carbonated cement powders are also highly susceptible. Low vegetation cover

(NDVI -0.19 to -0.13) is another major factor. The distance to rivers, particularly between 567.89 and 1140.24 meters, significantly affects flood risk. Depressions or convergent zones, indicated by curvature values of 0.65 to 9.60, are also important. Other key factors include low areas that accumulate water (TPI 0.49–5.25), zones with higher water accumulation (TWI 2.51–4.98), and areas

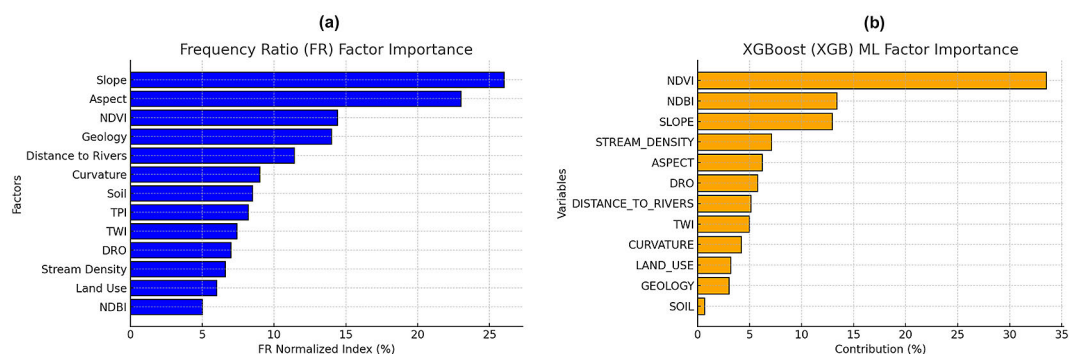


**Figure 6.** Comparison of factor importance in flood prediction across RF, XGBoost model and statistical method frequency ratio: (a) frequency ratio, (b) XGBoost model

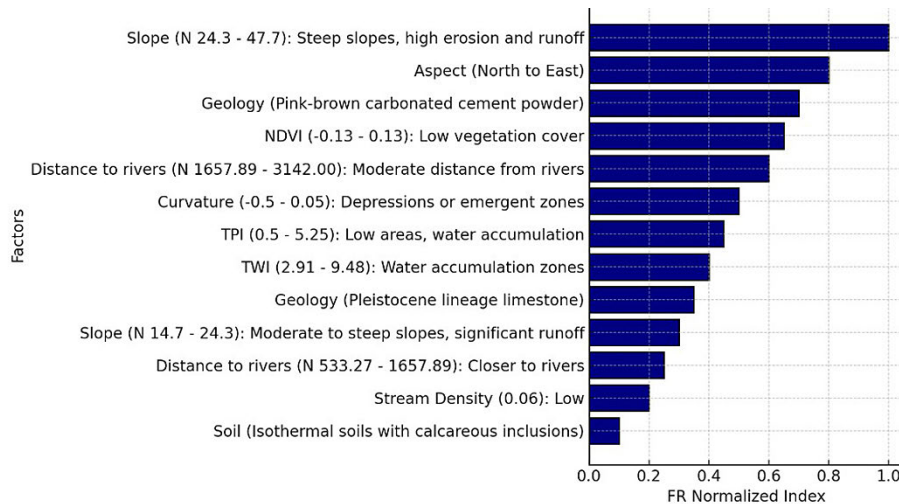


**Figure 7.** Relative contribution of factor classes to predictions using the FR method

with Paleocene beige limestone. Moderate to steep slopes (14.79–24.33%) with significant runoff, closer proximity to rivers (357.72–567.89 meters), stream density (0–0.67 km/km<sup>2</sup>), and specific soil types like isohumic soils with calsimagnesian inclusions further influence flood hazards.

In the analysis performed with XGBoost, the bar chart provides a clear picture of how different factors influence flood predictions using the XGBoost (XGB) algorithm. Steep slopes are the most significant contributors (24.33–47.73%), playing a key role in increasing runoff and erosion both critical drivers of flooding. Geological features, like pink-brown carbonated cement powders, also have a notable impact, showing how the makeup of the terrain affects flood Hazard. Additionally, regions with sparse vegetation (NDVI: 0.194–0.135) are highly influential, as low vegetation limits the land's ability to absorb water, leading to more surface runoff. Moderately important factors include the distance to rivers (567.89–1140.24 m), which shows that areas closer to water bodies are at higher risk, and terrain curvature (0.05–0.69), which identifies areas where water tends to collect, such as dips or rises in the land. Other factors in this category include Middle Quaternary geology and the topographical wetness index (TWI), both of which highlight zones where water naturally accumulates.

Urban land use (built-up areas), aspect (West to North), and stream density (0.67–1.20 km/km<sup>2</sup>) contribute less to flood dynamics but still play a role. Overall, the chart underscores that topographical and geological features are the primary drivers of flood risks, while proximity to water bodies and

land cover factors add valuable supporting insights. This analysis provides a well-rounded understanding of the elements that shape flood hazard.

#### Analysis of prediction score distributions

To evaluate the distribution of prediction scores and their ability to differentiate flood-prone areas, Histograms of prediction scores from the FR and XGBoost models were analyzed to assess their ability to differentiate flood-prone areas (Figure 8). The FR model's predictions were heavily concentrated near 1.0 in the training set, indicating a strong focus on areas identified as highly flood-prone. However, its outputs were largely binary, offering less granularity in risk differentiation. In contrast, XGBoost showed a bimodal distribution with peaks at 0.0 and 1.0, effectively separating low and high flood risks. The test set followed this trend with reduced extremes, demonstrating better generalization and avoiding overfitting. XGBoost's more nuanced probability distribution provides a detailed flood susceptibility map, capturing intermediate risk levels. While the FR model offers interpretability, XGBoost delivers finer differentiation, making it better suited for detailed flood risk assessments (Figure 9).

#### Urban flood hazard probability mapping

The representation of the likelihood of urban flooding provides a visual indication of flood risk within the city. Using the natural breaks (Jenks) (0–1) method in a GIS framework, the maps were divided into five levels of hazard: very low, low, moderate, high, and very high. A

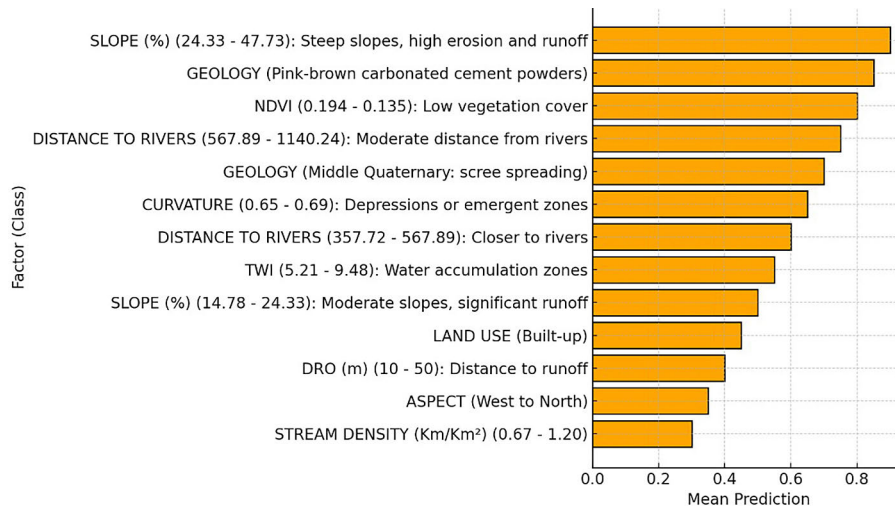


Figure 8. Relative contribution of factor classes to predictions using the XGBoost model

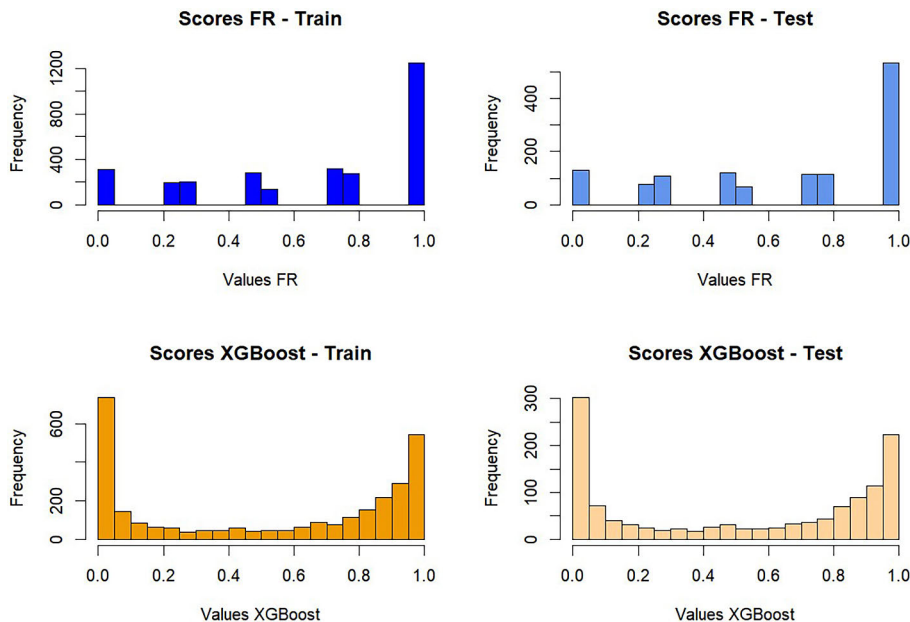


Figure 9. Analysis of prediction score distributions: FR and XGBoost models

detailed analysis demonstrates differences in the distribution of flood hazard categories across the two methods (XGBoost and FR). The two maps illustrate different approaches to flood hazard assessment. The map based on the FR method shows a balanced distribution of hazard categories across the study area. It features a smooth transition from “very low” risk (21.3%) to “very high” risk (11.3%), with notable representation in intermediate categories such as “moderate” (25.3%) and “high” (18.3%). This model is particularly useful for overall assessment and long-term flood management strategies, enabling

decision-makers to plan proportionate measures across the identified zones (Figure 10).

In contrast, the map generated using the XGBoost model highlights a predominance of “very low” risk areas (73.0%), while “low” (5.7%), “moderate” (4.3%), “high” (5.0%), and “very high” (12.0%) risk zones are less represented. High and very high-risk zones are concentrated in specific locations, often urban areas or vulnerable regions. This model emphasizes precise identification of extreme-risk areas, making it particularly valuable for targeted interventions and efficient allocation of resources for flood prevention. The

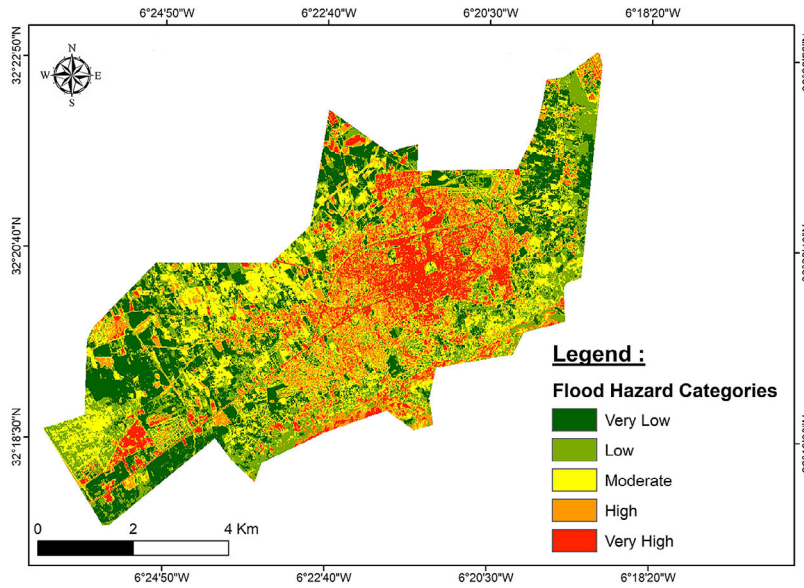


Figure 10. Flood hazard map generated by statistical method FR

FR map is ideal for comprehensive action plans, while the XGBoost map is better suited for operational responses in critical areas. Together, these approaches complement each other one offering a broad overview and the other refining the analysis for precise targeting (Figure 11, 12).

**Performance analysis**

The ROC curves presented in the Figure 13 depict the performance of the Frequency Ratio and XGBoost models in distinguishing between flooded and non-flooded areas for both the training (a), and testing (b) datasets. The AUC values

give the quantitative comparison of the models’ effectiveness.

The AUC for the XGBoost model in the training dataset is close to perfection at 99.85%, while FR presents a relative lower AUC of 89.2% (Fig. 13a), which demonstrates that the performances are relatively good, though much less precise than XGBoost. This wide difference in the performance between the two underpins the higher predictability enjoyed by XGBoost, thus benefiting from the nature of machine learning and thereby non-linear interaction.

On the testing set, model XGBoost retains a high performance with an AUC of 90.71%,

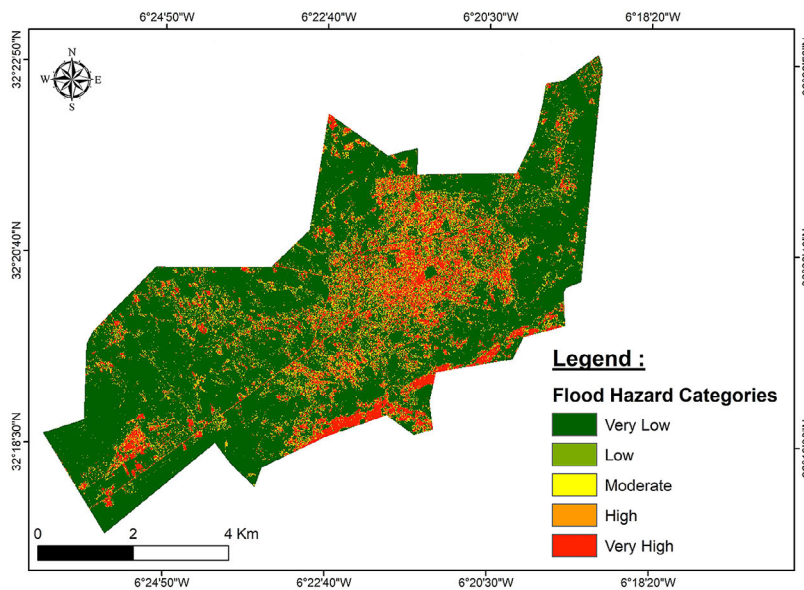
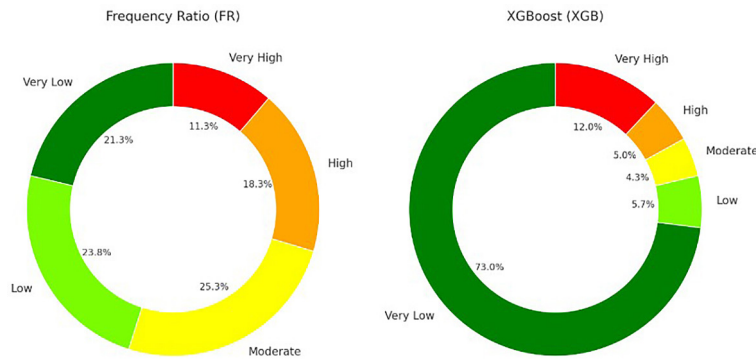


Figure 11. Flood hazard map generated by machine learning model XGBoost



**Figure 12.** Flood hazard zone distribution across frequency ratio method, and XGBoost machine learning model

confirming that the model generalizes well on unseen data. In contrast, FR has an AUC of only 86.1% (Fig. 13b), reflecting a slightly lower generalization capability. However, such reduction does not diminish in any sense the usefulness of predictions made by this model; the FR model, though useful in giving predictions, just lacks the robustness and reliability associated with XGBoost.

On the whole, from both analyses, XGBoost suits both datasets very well. Therefore, in the case where the application calls for high accuracy and generalization, it may serve as a better fit. FR suits cases with less complication and is better in carrying out speedy yet less complicated analyses. These differences between the two models constitute a good reference for deciding on an appropriate tool to deal with tasks related to flood prediction.

In terms of performance metrics (Figure 14), the results clearly show that the XGBoost model significantly outperforms the FR model across all key indicators, including accuracy, class

consistency (Kappa), MAE, and RMSE. XGBoost has an accuracy of 90.5% in training and 84.4% in testing, compared to 69% and 66.9% respectively for FR. In addition, XGBoost has strong consistency across classes, with Kappa values of 0.81 in training and 0.69 in testing, much higher than the 0.38 and 0.34 in the FR model. These results show that XGBoost is more reliable and stable in predicting flooded areas, offering predictions closer to true values and with reduced error. As a result, XGBoost is recommended for applications that require high accuracy, while FR can be used for faster and less demanding analyses.

## DISCUSSION

This study focuses on flood hazard assessment, a comparative analysis of two prominent methodological approaches, the FR method and the XGBoost model. It aims to underline their respective strengths while identifying the most

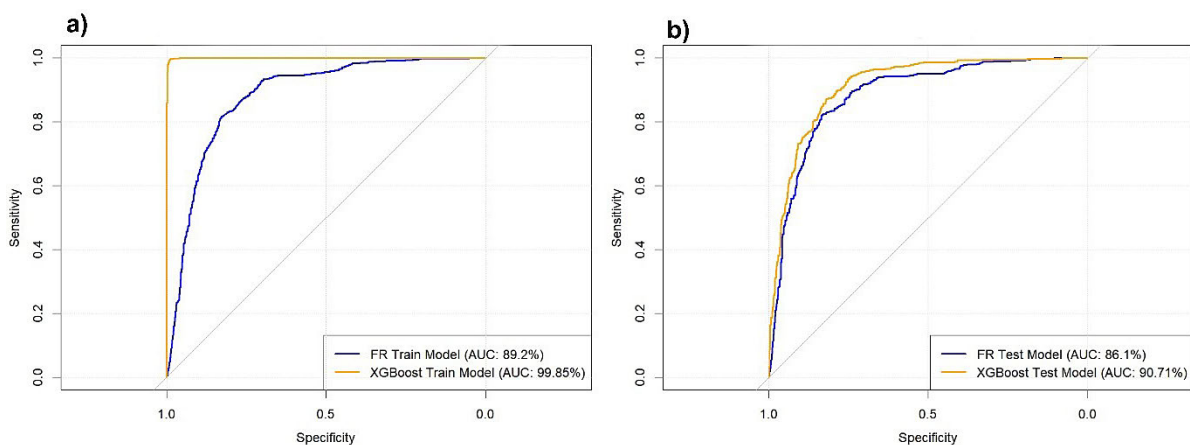


**Figure 13.** ROC curves for flood prediction models – comparison between FR and XGBoost: (a) training data performance (AUC: FR = 89.2%, XGBoost = 99.85%), (b) testing data performance (AUC: FR = 86.1%, XGBoost = 90.71%)



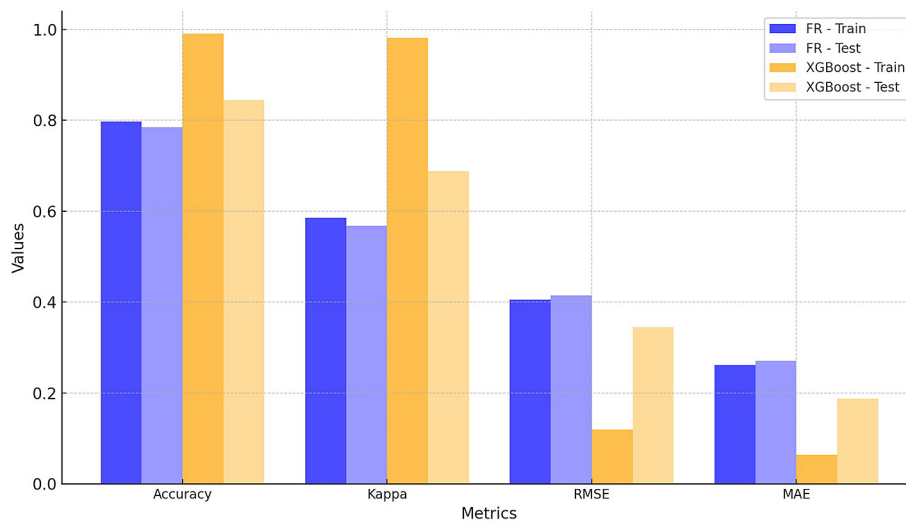


**Figure 14.** Bar chart comparing FR and XGBoost using multiple performance metrics – accuracy, mean absolute error (MAE) and root mean square error (RMSE) and Kappa

influential variables in predicting flood-prone areas. These approaches, which combine traditional techniques with advanced machine learning methods, offer complementary insights into flood risk and provide valuable tools for informed decision-making.

Comparing the XGBoost algorithm with the FR method highlights how both approaches offer valuable but slightly different perspectives on flood risk. Both agree that steep slopes (24.33–47.73%) play the biggest role in flooding by increasing runoff and erosion, making them critical in understanding flood dynamics. Similarly, areas with low vegetation cover (NDVI: 0.194–0.135 in XGB and -0.19 to -0.13 in FR) are highlighted by both methods, as sparse vegetation reduces the land's ability to absorb water, leading to more surface runoff. Proximity to rivers (567.89–1140.24 m) is another shared factor, with both models recognizing its influence on flood risk, particularly in areas near water bodies.

Where they differ, FR brings a more detailed focus on geographical features, such as the impact of positive curvature (0.65–9.60) and north-east-facing slopes, which can direct and concentrate water flow (Kaffas et al., 2022). Meanwhile, XGBoost provides a broader overview, ranking the importance of various factors in flood prediction. Together, these methods complement each other, with XGBoost excelling at quantifying factor contributions and FR offering a more nuanced look at specific geographical dynamics. By combining their strengths, we can gain a deeper understanding of flood risks and develop more

targeted mitigation strategies. The applicability of the FR model in various urban contexts has been further demonstrated in New Cairo, Egypt, where it achieved an AUC of 90.11% (Megahed et al., 2023), showcasing its effectiveness for rapid and resource-efficient flood susceptibility mapping. Thus, the FR method excels in producing quick and interpretable flood hazard maps, particularly suitable for preliminary assessments.

Conversely, the XGBoost model leverages its ability to model complex, nonlinear relationships between variables, delivering detailed and refined results. For example, a case study in Bahir Dar, Ethiopia, demonstrated its robustness with an AUC of 98%, identifying critical predictors such as proximity to rivers and drainage systems (Legesse et al., 2024). This model excels in capturing intricate variable interactions, offering high accuracy and detailed risk mapping (Wu et al., 2024). In Suqian City, China, XGBoost was shown to outperform Logistic Regression and Random Forest in precision and specificity for flood sensitivity assessment (Wu et al., 2024).

When comparing their performance, it becomes evident that XGBoost outperforms the FR method across all key metrics. XGBoost achieved an accuracy of 90.5% in training and 84.4% in testing, significantly higher than the 69% and 66.9% observed for FR. Similarly, the consistency between classes, measured by Kappa values, was superior in XGBoost, with scores of 0.81 in training and 0.69 in testing, compared to 0.38 and 0.34 for FR. Furthermore, XGBoost demonstrates reduced errors, as reflected in its lower MAE and

RMSE, translating to predictions that are more reliable and closer to actual values. This observation aligns with findings from Suqian City, where XGBoost demonstrated an AUC of 0.854 for test datasets, showcasing its robustness in predicting flood sensitivity (Wu et al., 2024).

Moreover, the flood hazard maps generated by these models highlight their differing approaches to risk assessment. The FR model presents a balanced risk distribution, transitioning gradually from low-risk areas (21.3%) to very high-risk zones (11.3%). This makes it effective for broad evaluations and long-term planning. The model's application in Greater Mumbai validated its efficiency in urban flood zoning using limited data (Ramesh and Iqbal, 2022). On the other hand, the XGBoost model emphasizes very high-risk areas (12.0%) while predominantly identifying very low-risk zones (73.0%), offering precision invaluable for targeted interventions and efficient resource allocation.

In conclusion, this comparative analysis underscores the complementary advantages of both models. The FR method is ideal for rapid, overarching analyses that guide strategic planning, while XGBoost excels in delivering detailed and precise risk mapping through its ability to model complex relationships. The integration of findings from Suqian City demonstrates how XGBoost's sophisticated modeling capabilities provide critical insights into urban flood risk. Combining these approaches offers a robust framework for comprehensive flood risk assessment, optimizing resource management and prevention strategies. This ensures that both global perspectives and localized details are effectively addressed.

## CONCLUSIONS

This comparative study underscores the complementary advantages of the FR method and the XGBoost model in flood hazard assessment. The FR method's simplicity and reliance on geographical variables make it an excellent tool for preliminary analyses, especially in data-scarce regions or during rapid assessments. Conversely, the XGBoost model demonstrates superior accuracy and precision by capturing complex, nonlinear relationships between variables, integrating both natural and anthropogenic factors. Its robustness in detailed mapping and risk differentiation is particularly evident in urbanized

and data-rich contexts. Together, these methods provide a holistic approach to flood risk assessment, balancing rapid insights with detailed analysis for strategic and localized decision-making. The FR model's utility has been validated in urban contexts like New Cairo and Greater Mumbai, where it provided interpretable results for broad-scale evaluations. Similarly, XGBoost has demonstrated exceptional performance in studies such as Bahir Dar and Suqian City, highlighting its ability to prioritize high-risk areas and allocate resources efficiently. While XGBoost outperforms FR across key metrics, including accuracy, Kappa values, and error reduction, the FR method remains highly relevant for quick hazard mapping and strategic planning. Despite the strengths of both models, this study acknowledges several limitations. The XGBoost model's performance depends heavily on the availability of high-quality datasets, which may not be accessible in underdeveloped regions or during emergency scenarios. Additionally, its computational complexity, including intensive parameter tuning, can restrict its usability in real-time or resource-limited environments. Conversely, the FR method's reliance on linear assumptions and variable independence may oversimplify the complex dynamics of flood hazards. Both models also face challenges in generalizability. Their performance is often sensitive to the specific geographic and climatic characteristics of the study area, potentially limiting their applicability across diverse regions. Furthermore, validation metrics such as AUC and Kappa values, while useful, may not fully account for long-term reliability under changing environmental conditions, such as urban expansion or climate change. To address these limitations, future research should explore the integration of FR and XGBoost into a hybrid framework that combines the strengths of both approaches. For instance, FR can provide a rapid, initial assessment, while XGBoost delivers detailed and precise risk mapping. Enriching datasets with real-time information from satellite imagery, IoT sensors, and crowd-sourced data can further enhance the accuracy and applicability of these models. Dynamic models that account for temporal changes in land use, climate, and hydrology should also be developed to improve predictions under evolving conditions. Expanding comparative analyses to include other advanced machine learning models, such as random forests or deep learning, may uncover additional insights into flood hazard modeling.

Moreover, the development of user-friendly, automated tools that integrate GIS with machine learning could bridge the gap between research and practical disaster management applications. Finally, testing models under various scenarios, such as extreme rainfall or urbanization, can validate their robustness and reliability in forecasting future risks. By addressing these limitations and pursuing these perspectives, future research can contribute to more comprehensive, adaptable, and effective flood risk management strategies.

### Acknowledgments

The authors express their sincere gratitude to the researchers supporting the PRIMA Resilink project for their invaluable support of this research article. In addition, they sincerely appreciate the anonymous reviewers for their insightful and constructive comments.

### REFERENCES

1. Abdrabo, K. I., Kantoush, S. A., Saber, M., Sumi, T., Habiba, O. M., Elleithy, D., & Elboshy, B. (2020). Integrated Methodology for Urban Flood Risk Mapping at the Microscale in Ungauged Regions : A Case Study of Hurghada, Egypt. *Remote Sensing*, *12*(21), 3548. <https://doi.org/10.3390/rs12213548>
2. Alipour, A., Ahmadalipour, A., Abbaszadeh, P., & Moradkhani, H. (2020). Leveraging machine learning for predicting flash flood damage in the Southeast US. *Environmental Research Letters*, *15*(2), 024011. <https://doi.org/10.1088/1748-9326/ab6edd>
3. Allouche, O., Tsoar, A., & Kadmon, R. (2006). Assessing the accuracy of species distribution models : Prevalence, kappa and the true skill statistic (TSS). *Journal of Applied Ecology*, *43*, 1223–1232. <https://doi.org/10.1111/J.1365-2664.2006.01214.X>
4. Almouctar, M. A. S., Wu, Y., An, S., Yin, X., Qin, C., Zhao, F., & Qiu, L. (2024). Flood risk assessment in arid and semi-arid regions using Multi-criteria approaches and remote sensing in a data-scarce region. *Journal of Hydrology: Regional Studies*, *54*, 101862. <https://doi.org/10.1016/j.ejrh.2024.101862>
5. Anaya-Romero, M., Abd-Elmabod, S. K., Muñoz-Rojas, M., Castellano, G., Ceacero, C. J., Alvarez, S., Méndez, M., & De la Rosa, D. (2015). Evaluating Soil Threats Under Climate Change Scenarios in the Andalusia Region, Southern Spain. *Land Degradation & Development*, *26*(5), 441–449. <https://doi.org/10.1002/ldr.2363>
6. Antzoulatos, G., Kouloglou, I.-O., Bakratsas, M., Moutzidou, A., Gialampoukidis, I., Karakostas, A., Lombardo, F., Fiorin, R., Norbiato, D., Ferri, M., Symeonidis, A., Vrochidis, S., & Kompatsiaris, I. (2022). Flood Hazard and Risk Mapping by Applying an Explainable Machine Learning Framework Using Satellite Imagery and GIS Data. *Sustainability*, *14*(6), 3251. <https://doi.org/10.3390/su14063251>
7. Arabameri, A., Chandra Pal, S., Costache, R., Saha, A., Rezaie, F., Seyed Danesh, A., Pradhan, B., Lee, S., & Hoang, N.-D. (2021). Prediction of gully erosion susceptibility mapping using novel ensemble machine learning algorithms. *Geomatics, Natural Hazards and Risk*, *12*(1), 469–498. <https://doi.org/10.1080/19475705.2021.1880977>
8. Arabameri, A., Pal, S., Costache, R.-D., Saha, A., Rezaie, F., Danesh, A., Pradhan, B., Lee, S., & Hoang, N.-D. (2021). Prediction of gully erosion susceptibility mapping using novel ensemble machine learning algorithms. *Geomatics, Natural Hazards and Risk*, 469–498. <https://doi.org/10.1080/19475705.2021.1880977>
9. Atefi, M. R., & Miura, H. (2022). Detection of flash flood inundated areas using relative difference in NDVI from Sentinel-2 Images : A case study of the August 2020 Event in Charikar, Afghanistan. *Remote Sensing*, *14*(15), 3647. <https://doi.org/10.3390/rs14153647>
10. Avand, M., Kuriqi, A., Khazaei, M., & Ghorbanzadeh, O. (2022). DEM resolution effects on machine learning performance for flood probability mapping. *Journal of Hydro-Environment Research*, *40*, 1-16. <https://doi.org/10.1016/j.jher.2021.10.002>
11. Barakat, A., Ennaji, W., Krimissa, S., & Bouzaid, M. (2020). Heavy metal contamination and ecological-health risk evaluation in peri-urban wastewater-irrigated soils of Beni-Mellal city (Morocco). *International Journal of Environmental Health Research*, *30*(4), 372–387. <https://doi.org/10.1080/09603123.2019.1595540>
12. Bechkit, M. A., Boufekane, A., Busico, G., Lama, G. F. C., Mouhoub, F. C., Aichaoui, M., Arrache, K., & Bourouis, S. (2024). Seawater intrusion mapping using geophysical methods, piezometry, and hydrochemical data analysis : Application in the Coastal Aquifer of Nador Wadi Plain in Tipaza (Algeria). *Pure and Applied Geophysics*. <https://doi.org/10.1007/s00024-024-03565-2>
13. Beshir, A. A., & Song, J. (2021). Urbanization and its impact on flood hazard: The case of Addis Ababa, Ethiopia. *Natural Hazards*, *109*(1), 1167–1190. <https://doi.org/10.1007/s11069-021-04873-9>
14. Bogale, A. (2021). Morphometric analysis of a drainage basin using geographical information system in Gilgel Abay watershed, Lake Tana Basin, upper Blue Nile Basin, Ethiopia. *Applied Water Science*, *11*(7), 122. <https://doi.org/10.1007/>

- s13201-021-01447-9
15. Bouramtane, T., Hilal, H., Rezende-Filho, A. T., Bouramtane, K., Barbiero, L., Abraham, S., Valles, V., Kacimi, I., Sanhaji, H., Torres-Rondon, L., De Castro, D. D., Vieira Santos, J. D. C., Ouardi, J., Beqqali, O. E., Kassou, N., & Morarech, M. (2022). Mapping gully erosion variability and susceptibility using remote sensing, multivariate statistical analysis, and machine learning in south Mato Grosso, Brazil. *Geosciences*, 12(6), 235. <https://doi.org/10.3390/geosciences12060235>
  16. Cea, L., & Costabile, P. (2022). Flood risk in urban areas: Modelling, management and adaptation to climate change. A Review. *Hydrology*, 9(3), 50. <https://doi.org/10.3390/hydrology9030050>
  17. Chen, Y., Liu, R., Barrett, D., Gao, L., Zhou, M., Renzullo, L., & Emelyanova, I. (2015). A spatial assessment framework for evaluating flood risk under extreme climates. *Science of The Total Environment*, 538, 512–523. <https://doi.org/10.1016/j.scitotenv.2015.08.094>
  18. Crimaldi, M., & Lama, G. F. C. (2021). *Impact of riparian plants biomass assessed by UAV-acquired multispectral images on the hydrodynamics of vegetated streams*. 1157–1161. Scopus.
  19. Eini, M., Kaboli, H. S., Rashidian, M., & Hedayat, H. (2020). Hazard and vulnerability in urban flood risk mapping : Machine learning techniques and considering the role of urban districts. *International Journal of Disaster Risk Reduction*, 50, 101687. <https://doi.org/10.1016/j.ijdr.2020.101687>
  20. Haghizadeh, A., Siahkamari, S., Haghiabi, A. H., & Rahmati, O. (2017). Forecasting flood-prone areas using Shannon’s entropy model. *Journal of Earth System Science*, 126(3), 39. <https://doi.org/10.1007/s12040-017-0819-x>
  21. Ibrahim, M., Huo, A., Ullah, W., Ullah, S., Ahmad, A., & Zhong, F. (2024). Flood vulnerability assessment in the flood prone area of Khyber Pakhtunkhwa, Pakistan. *Frontiers in Environmental Science*, 12. <https://doi.org/10.3389/fenvs.2024.1303976>
  22. Ismaili, M., Krimissa, S., Namous, M., Boudhar, A., Edahbi, M., Lebrini, Y., Htitiou, A., Maimouni, S., & Benabdelouahab, T. (2024). Mapping soil suitability using phenological information derived from MODIS time series data in a semi-arid region : A case study of Khouribga, Morocco. *Helijon*, 10, e24101. <https://doi.org/10.1016/j.helijon.2024.e24101>
  23. Ismaili, M., Krimissa, S., Namous, M., Htitiou, A., Abdelrahman, K., Fnais, M. S., Lhissou, R., Eloudi, H., Faouzi, E., & Benabdelouahab, T. (2023). Assessment of soil suitability using machine learning in arid and semi-arid regions. *AGRONOMY-BASEL*, 13(1). <https://doi.org/10.3390/agronomy13010165>
  24. Janizadeh, S., Chandra Pal, S., Saha, A., Chowdhuri, I., Ahmadi, K., Mirzaei, S., Mosavi, A. H., & Tiefenbacher, J. P. (2021). Mapping the spatial and temporal variability of flood hazard affected by climate and land-use changes in the future. *Journal of Environmental Management*, 298, 113551. <https://doi.org/10.1016/j.jenvman.2021.113551>
  25. Kaffas, K., Papaioannou, G., Varlas, G., Al Sayah, M. J., Papadopoulos, A., Dimitriou, E., Katsafados, P., & Righetti, M. (2022). Forecasting soil erosion and sediment yields during flash floods : The disastrous case of Mandra, Greece, 2017. *Earth Surface Processes and Landforms*, 47(7), 1744–1760. <https://doi.org/10.1002/esp.5344>
  26. Khan, M. S., Ullah, S., & Chen, L. (2021). Comparison on land-use/land-cover indices in explaining land surface temperature variations in the city of Beijing, China. *Land*, 10(10), Article 10. <https://doi.org/10.3390/land10101018>
  27. Leggesse, E. S., Derseh, W. A., Zimale, F. A., Tilahun, S. A., & Meshesha, M. A. (2024). Urban flash flood hazard mapping using machine learning, Bahir Dar, Ethiopia. *Journal of Hydroinformatics*, 26(9), 2124–2145. <https://doi.org/10.2166/hydro.2024.277>
  28. Lense, G. H. E., Lämmle, L., Ayer, J. E. B., Lama, G. F. C., Rubira, F. G., & Mincato, R. L. (2023). Modeling of Soil Loss by Water Erosion and Its Impacts on the Cantareira System, Brazil. *Water*, 15(8), Article 8. <https://doi.org/10.3390/w15081490>
  29. Luong, T. T., Pöschmann, J., Kronenberg, R., & Bernhofer, C. (2021). Rainfall Threshold for Flash Flood Warning Based on Model Output of Soil Moisture : Case Study Wernersbach, Germany. *Water*, 13(8), 1061. <https://doi.org/10.3390/w13081061>
  30. Mahmoud, S. H., & Gan, T. (2018). Urbanization and climate change implications in flood risk management : Developing an efficient decision support system for flood susceptibility mapping. *The Science of the total environment*, 636, 152–167. <https://doi.org/10.1016/j.scitotenv.2018.04.282>
  31. Megahed, H. A., Abdo, A. M., AbdelRahman, M. A. E., Scopa, A., & Hegazy, M. N. (2023). Frequency ratio model as tools for flood susceptibility mapping in urbanized areas : A case study from Egypt. *Applied Sciences*, 13(16), 9445. <https://doi.org/10.3390/app13169445>
  32. Nguyen, B. D., Minh, D. T., Ahmad, A., & Nguyen, Q. L. (2020). The role of relative slope length in flood hazard mapping using ahp and gis (Case Study : Lam River Basin, Vietnam). *Geography, Environment, Sustainability*, 13(2), 115–123. <https://doi.org/10.24057/2071-9388-2020-48>
  33. Paul, E., Harrison, C., Satchell, L., Goff, L. L., & O’Callaghan, K. (2022). Novel approaches to healthcare-associated infection surveillance validation using Cohen’s Kappa. *American Journal of Infection Control*, 50(7, Supplement), S7. <https://doi.org/10.1016/j.ajic.2022.03.129>

34. Peng, J., Kim, M., & Sung, K. (2020). Yield prediction modeling for sorghum-sudangrass hybrid based on climatic, soil, and cultivar data in the Republic of Korea. *Agriculture-Basel*, 10(4). <https://doi.org/10.3390/agriculture10040137>
35. Pham, B. T., Jaafari, A., Prakash, I., Singh, S. K., Quoc, N. K., & Bui, D. T. (2019). Hybrid computational intelligence models for groundwater potential mapping. *Catena*, 182, 104101. <https://doi.org/10.1016/j.catena.2019.104101>
36. Pirone, D., Cimorelli, L., & Pianese, D. (2024). The effect of flood-mitigation reservoir configuration on peak-discharge reduction during preliminary design. *Journal of Hydrology: Regional Studies*, 52, 101676. <https://doi.org/10.1016/j.ejrh.2024.101676>
37. Rahman, M., Ningsheng, C., Mahmud, G. I., Islam, M. M., Pourghasemi, H. R., Ahmad, H., Habumugisha, J. M., Washakh, R. M. A., Alam, M., Liu, E., Han, Z., Ni, H., Shufeng, T., & Dewan, A. (2021). Flooding and its relationship with land cover change, population growth, and road density. *Geoscience Frontiers*, 12(6), 101224. <https://doi.org/10.1016/j.gsf.2021.101224>
38. Rahmati, O., Pourghasemi, H. R., & Zeinivand, H. (2016). Flood susceptibility mapping using frequency ratio and weights-of-evidence models in the Golastan Province, Iran. *Geocarto International*, 31(1), 42–70. <https://doi.org/10.1080/10106049.2015.1041559>
39. Raja, N. B., Çiçek, I., Türkoğlu, N., Aydın, O., & Kawasaki, A. (2017). Landslide susceptibility mapping of the Sera River Basin using logistic regression model. *Natural Hazards*, 85(3), 1323–1346. <https://doi.org/10.1007/s11069-016-2591-7>
40. Ramesh, V., & Iqbal, S. S. (2022). Urban flood susceptibility zonation mapping using evidential belief function, frequency ratio and fuzzy gamma operator models in GIS : A case study of Greater Mumbai, Maharashtra, India. *Geocarto International*, 37(2), 581–606. <https://doi.org/10.1080/10106049.2020.1730448>
41. Ren, H., Pang, B., Bai, P., Zhao, G., Liu, S., Liu, Y., & Li, M. (2024). Flood susceptibility assessment with random sampling strategy in ensemble learning (RF and XGBoost). *Remote Sensing*, 16(2), Article 2. <https://doi.org/10.3390/rs16020320>
42. Salimi, M., & Al-Ghamdi, S. G. (2020). Climate change impacts on critical urban infrastructure and urban resiliency strategies for the Middle East. *Sustainable Cities and Society*, 54, 101948. <https://doi.org/10.1016/j.scs.2019.101948>
43. Soussa, H. (2010). *Integrated Flood and Drought Management for Sustainable Development in the Nile Basin*. [https://www.academia.edu/70522279/Integrated\\_Flood\\_and\\_Drought\\_Management\\_for\\_Sustainable\\_Development\\_in\\_the\\_Nile\\_Basin](https://www.academia.edu/70522279/Integrated_Flood_and_Drought_Management_for_Sustainable_Development_in_the_Nile_Basin)
44. Talha, S., Akhssas, A., Aarab, A., Aabi, A., & Berkat, B. (2025). Enhancing flash flood risk prediction : A case study from the Assaka watershed, Guelmim region, Southwestern Morocco. *Ecological Engineering & Environmental Technology*, 26(1), 8–28. <https://doi.org/10.12912/27197050/195227>
45. Taromideh, F., Fazloulou, R., Choubin, B., Emadi, A., & Berndtsson, R. (2022). Urban Flood-Risk Assessment : Integration of Decision-Making and Machine Learning. *Sustainability*, 14(8), 4483. <https://doi.org/10.3390/su14084483>
46. Tehrany, M. S., Jones, S., & Shabani, F. (2019). Identifying the essential flood conditioning factors for flood prone area mapping using machine learning techniques. *CATENA*, 175, 174–192. <https://doi.org/10.1016/j.catena.2018.12.011>
47. Winzeler, H. E., Owens, P. R., Read, Q. D., Libohova, Z., Ashworth, A., & Sauer, T. (2022). Topographic wetness index as a proxy for soil moisture in a hillslope catena : Flow Algorithms and Map Generalization. *Land*, 11(11), Article 11. <https://doi.org/10.3390/land11112018>
48. Wu, Y., Zhang, Z., Qi, X., Hu, W., & Si, S. (2024). Prediction of flood sensitivity based on Logistic Regression, eXtreme Gradient Boosting, and Random Forest modeling methods. *Water Science & Technology*, 89(10), 2605–2624. <https://doi.org/10.2166/wst.2024.146>
49. Yalcin, A., Reis, S., Aydinoglu, A. C., & Yomralioglu, T. (2011). A GIS-based comparative study of frequency ratio, analytical hierarchy process, bivariate statistics and logistics regression methods for landslide susceptibility mapping in Trabzon, NE Turkey. *CATENA*, 85(3), 274–287. <https://doi.org/10.1016/j.catena.2011.01.014>
50. Yang, L., He, X., Shen, F., Zhou, C., Zhu, A.-X., Gao, B., Chen, Z., & Li, M. (2020). Improving prediction of soil organic carbon content in croplands using phenological parameters extracted from NDVI time series data. *Soil and Tillage Research*, 196, 104465. <https://doi.org/10.1016/j.still.2019.104465>